Supplementary Information for

Growth-Controlled $NiCo_2S_4$ Nanosheet Arrays with Self-Decorated Nanoneedles for High-Performance Pseudocapacitors

Liyang Lin[a,b¶], Jianlin Liu[a,c¶], Tianmo Liu[b*], Jinghua Hao[a,b], Kemeng Ji[a],Rong Sun[a], Wen Zeng[b], Zhongchang Wang[a*]

[a]*Advanced Institute for Materials Research, Tohoku University, 2-1-1 Katahira, Aoba-ku, Sendai 980-8577, Japan*

[b]*College of Materials Science and Engineering, Chongqing University, Chongqing 400030, China*

[c]*Department of Applied Physics, Chongqing University, Chongqing 400044, China*

Figure S1

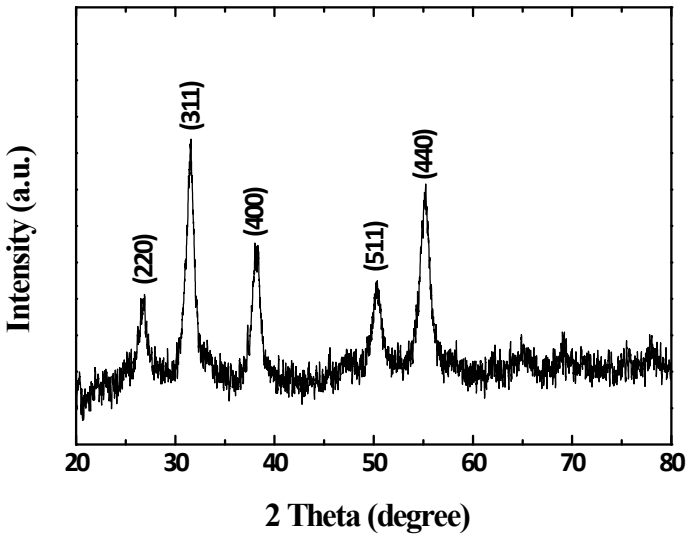

Fig. S1 XRD pattern for the sample SS_0 powders scraped from Ni foam.

Figure S2

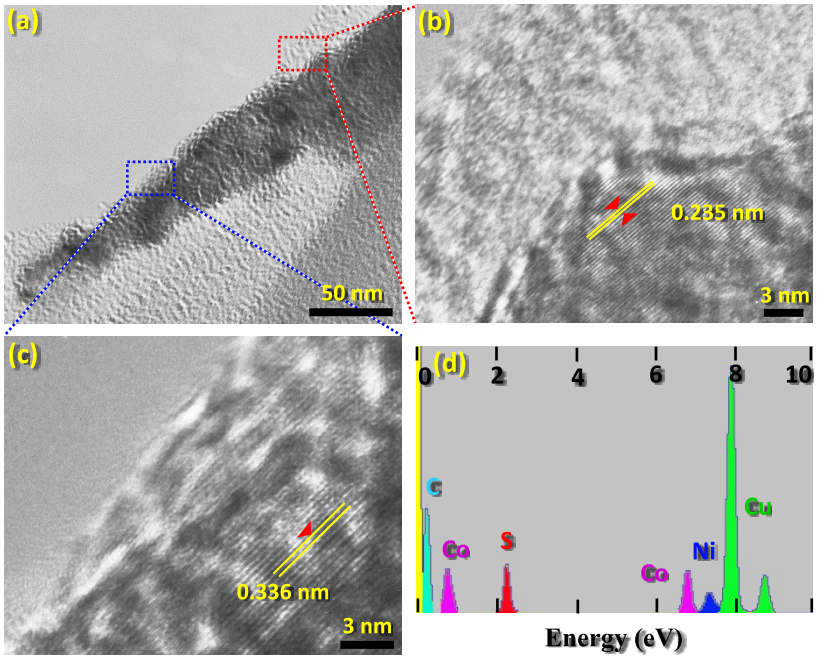

Fig. S2 TEM images and EDS spectra for an individual nanoneedles detached from the nanosheets in the $NiCo_2S_4$ sample SS_0.

Figure S3

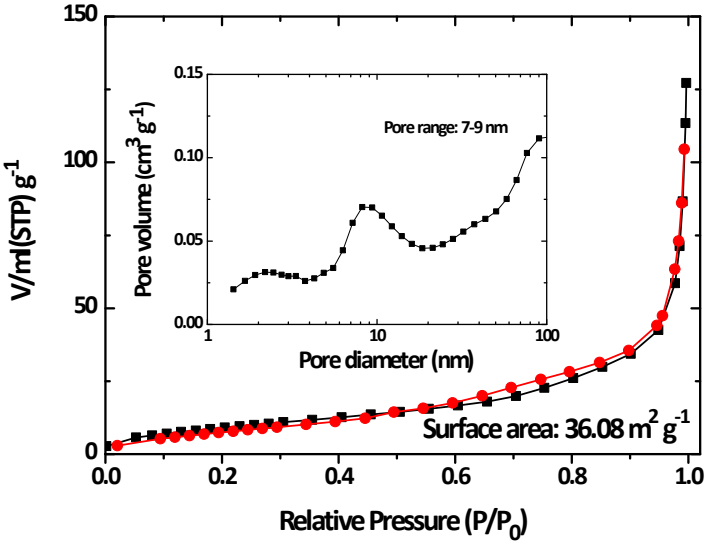

Fig. S3 N_2 adsorption-desorption isotherm and pore size distribution curves of the $NiCo_2S_4$ sample SS_0 powders scraped from the substrate.

Figure S4

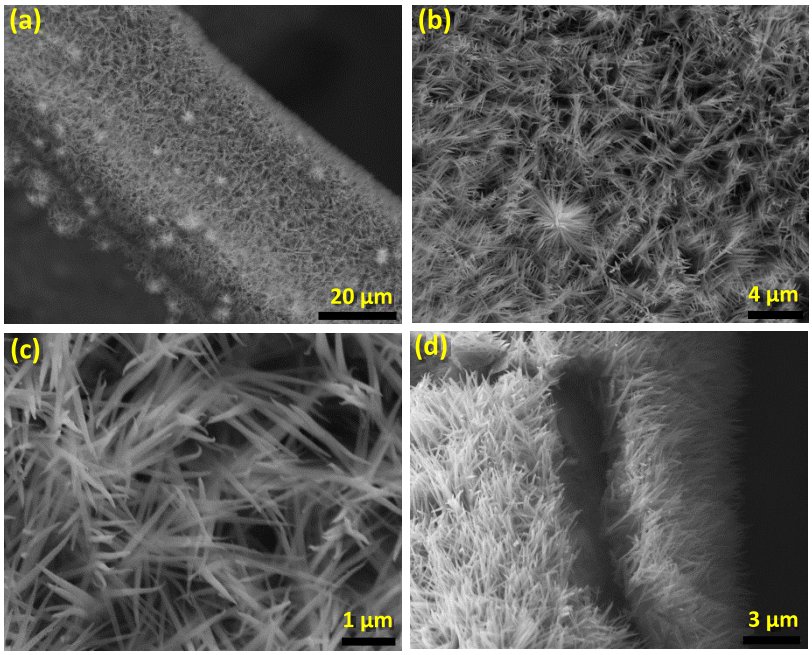

Fig. S4 SEM images of the $NiCo_2S_4$ sample synthesized by replacing NH_4F with NH_4Cl during the reaction.

Figure S5

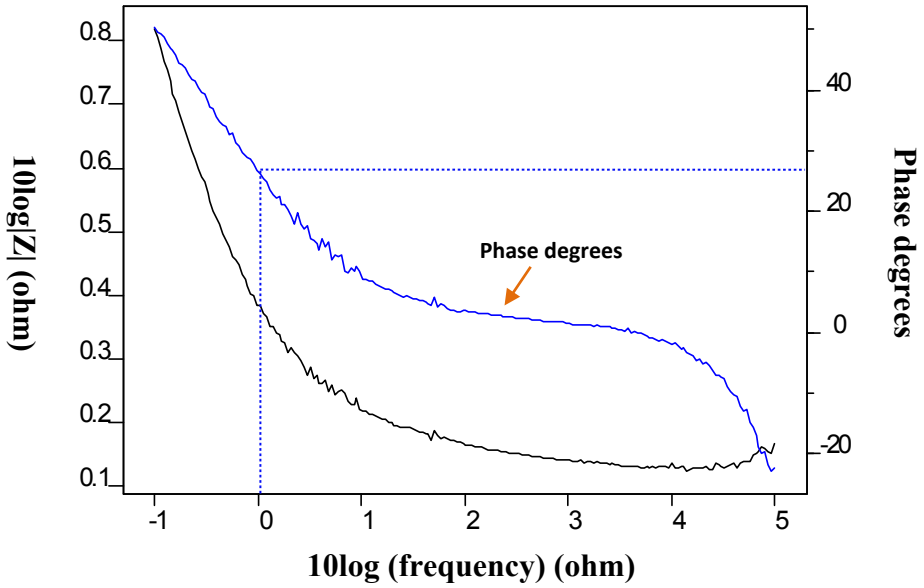

Fig. S5 Phase degrees as a function of frequency for the electrode SS_0.

Figure S6

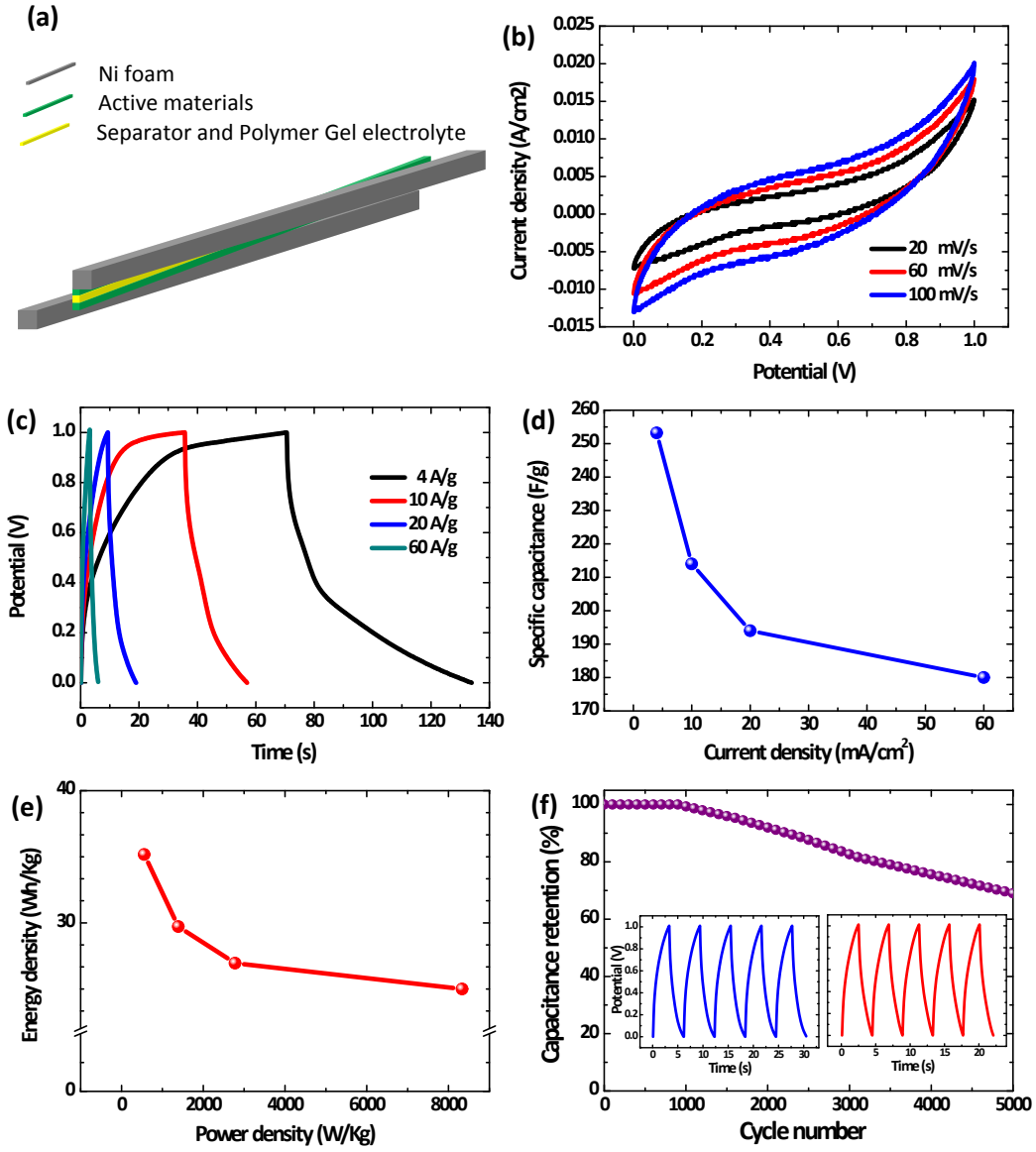

Fig. S6 (a) Schematic illustration of the sample SS_0 symmetric supercapacitor. (b) CV curves of the SS_0 device at various scan rates from 20 to 100 mVs^{-1} measured between 0 and 1.0 V. (c) GCD curves at various current densities. (d) The specific capacitance as a function of current density. (e) Ragone plot showing energy and power densities of the symmetric supercapacitor. (f) Cycling stability of symmetric supercapacitor at a current density of 20 Ag^{-1}. The insets show the first and the last five GCD curves.